

## CAAP Quarterly Report

[03/27/2024]

*Project Name: "All-in-One Multifunctional Cured-In-Place Structural Liner for Rehabilitating of Aging Cast Iron Pipelines"*

*Contract Number: 693JK32250009CAAP*

*Prime University: North Dakota State University*

*Prepared By: [Ying Huang, [ying.huang@ndsu.edu](mailto:ying.huang@ndsu.edu), 701-231-7651]*

*Reporting Period: [12/28/2023 – 03/27/2024]*

### Project Activities for Reporting Period:

In the 5<sup>th</sup> quarterly report, Tasks 2.1, 2.2, 3.1, 3.3, 3.4, 4.1, 4.2, and 5.1 were carried out as proposed. In this quarter (Quarter 6), the research team has consistent progress on selected tasks. The summaries of the key activities completed during the sixth reporting period are provided below.

**Task 2.1** Preparation of Vitrimers Epoxy Resins, Characterization, and Optimization of the Processing and Curing Conditions (80%): In the last report, the 1:1 formulation self-healing resin showed the best overall properties; therefore, it was selected by the research team (Dr. Long Jiang and Austin Knight, Ph. D. student from NDSU) to performed a further investigation. The study is divided into two main sections: the first one examined the rate of UV curing through a commercial liner, and the second one investigated the integration of nanoparticles into self-healing polymers; the key findings are presented below:

- (1) Influence of Liner on UV Curing Process: The curing rate of the optimal formulation, 1:1, was determined with and without the presence of the cure-in-place liner. Hardness measurements were conducted using a Shore D Durometer at various durations of UV curing. Subsequently, resin was dispensed into a silicon tensile test mold, with the cut liner placed on top. Results initially showed a slightly lower curing rate; however, hardness eventually reached levels comparable to samples without the liner (neat), suggesting that the liner minimally hinders adhesive curing once the duration exceeds 10 minutes, as shown in Figure 1 (c).

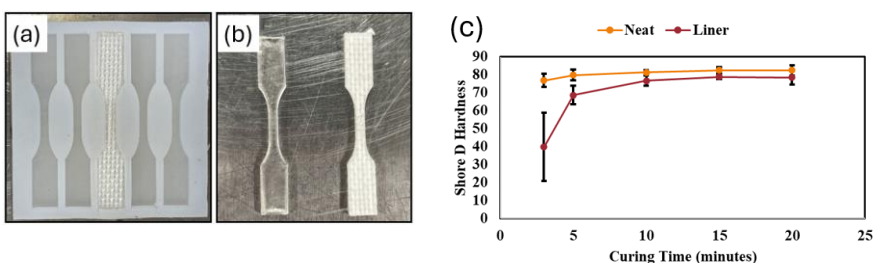


Figure 1. (a) (b) The resin in the silicon mold and the cut liner, and (c) hardness of the neat and liner covered sample after UV-curing.

**Task 2.2** Investigating Self-healing and Mechanical Properties of Vitrimers Epoxy Resins (50%): The research team (Dr. L. Jiang, Dr. Y. Huang, and Austin Knight, Ph. D. student from NDSU) investigated the influence of adding nanoparticles on self-healing properties of the selected 1:1 formulation self-healing polymer, and the results are presented below:

- (1) Self-Healing in UV-Cured Resin Nanoparticle Coatings: Coatings with uniform thickness were incised through their entire thickness using a razor blade to ensure consistent cut profiles across samples. The dimensions of each cut, including depth and profile, were assessed with a KEYENCE microscope both prior to and subsequent to the healing process. Healing was achieved by subjecting the coatings to a hot press at 180°C and 500 lbs. pressure for a duration of 10 minutes. To calculate

the average repair efficacy and its standard deviation, multiple incisions were made in each sample, with measurements taken before and after the healing process (Figure 2). The groups showing successful curing included those with 0.1 and 0.5 ND, and 0.1 GNP, with all formulations exhibiting an average repair ratio between 93.5-94.5%, excluding the 0.1% ND formulation, which demonstrated a repair ratio of 72%. The lower repair ratio in the 0.1% ND sample is attributed to an inconsistent coating thickness, which led to uneven heating; only the thickest regions at the top and bottom of the substrate made effective contact with the hot plates, resulting in more significant healing in those areas. Figure 3 presents profile images of the cuts both before and after the healing process, corroborating the measured depth values.

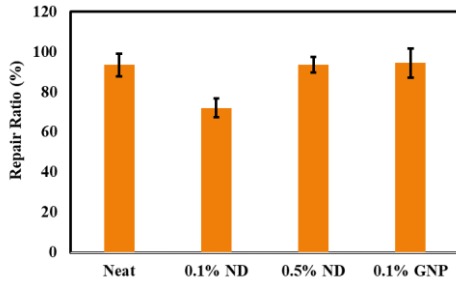


Figure 2. Repair ratio based on change in depth of the cut for the neat, 0.1% ND, 0.5% ND, and 0.1% GNP formulation. *Note: Concentrations of 0.1 to 1.0 wt.% for CNT, GNP, and ND were tested. All CNT samples and GNP samples at 0.5% and 1.0% concentrations impeded the UV-curing process, likely due to nanoparticles blocking UV light, preventing full curing. Successful curing was achieved with 0.1 and 0.5 ND, and 0.1 GNP samples.*

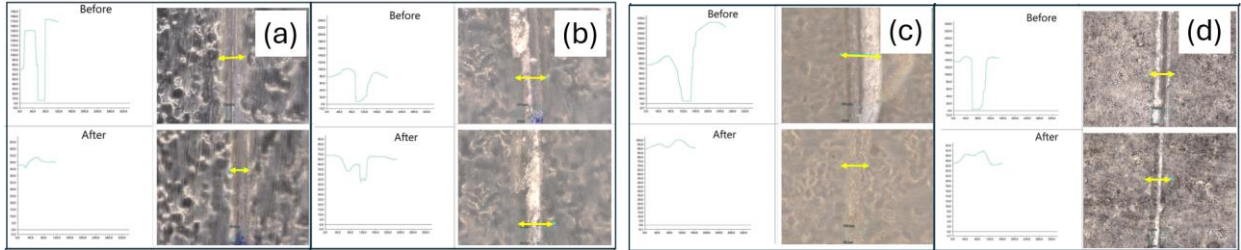


Figure 3. Profile images of before and after healing the (a) neat 1:1 formulation, and 1:1 formulation with (b) 0.1% ND. (c) 0.5% ND, and (d) 0.5% GNP.

**Task 3.1 High Mechanical Performance (70%):** During this reporting period, the research team (Dr. Ying Huang, Dr. Xingyu Wang, and Muhammad Imran Khan, Master student from NDSU) conducted an experimental study on nanoparticle reinforcement on the neat epoxy. The key findings are provided below:

- (1) Continue Investigation on Carboxymethyl Cellulose (CMC) Functionalization for Nanoparticles: The previous report explored a novel functionalization method employing CMC to enhance the dispersion of nanofillers and assess the mechanical characteristics of the nanocomposite. This investigation has been extended to include evaluations of abrasion and adhesion properties, which are illustrated in Figure 4. The results clearly demonstrate significant enhancements in both abrasion resistance and substrate adhesion for all nanoparticles functionalized with CMC, with ND exhibiting the most substantial overall improvement.

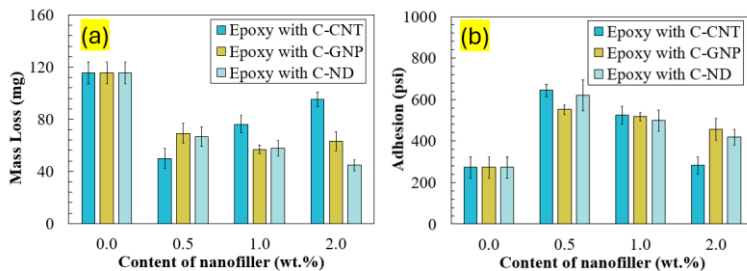


Figure 4. (a) Abrasion resistance and (b) adhesion/bonding to substrate of samples reinforced by CMC modified CNT, GNP, and ND.

**Task 3.3.** Reducing the Permeability and Investigating the Interfacial Bonding Chemical Analysis (50%): Previously, the research team (Dr. Liangliang Huang, Qiuhaio Chang, Ph. D. student from University of Oklahoma) constructed three different simple nanopores and evaluated hydrogen diffusion behavior with those models. For this reporting period, we continued investigated the pressure and confinement effects on the diffusion process; meanwhile, in alignment with the work on self-healing polymers, we have initiated the development of vitrimer models, and started with a non-reactive vitrimer model.

- (1) Pressure and Confinement Effects on Diffusion Process of H<sub>2</sub>: Figure 5 shows that at 20 atm, self-diffusion coefficients range from  $\sim 3.5 \times 10^{-6}$  m<sup>2</sup>/s to  $\sim 6.5 \times 10^{-6}$  m<sup>2</sup>/s in kaolinite pores and from  $\sim 5.5 \times 10^{-6}$  m<sup>2</sup>/s to  $\sim 7.0 \times 10^{-6}$  m<sup>2</sup>/s in graphene pores of 2 nm to 20 nm, respectively. The values agree with experimental data for H<sub>2</sub> transport on graphite surfaces, on the order of 10<sup>-7</sup>-10<sup>-6</sup> m<sup>2</sup>/s. As pore size increases, self-diffusion coefficients begin to approach that of bulk H<sub>2</sub>. In the case of kaolinite, the increase in self-diffusion coefficient from the 2 nm pore to bulk H<sub>2</sub> follows a somewhat linear trend. However, for graphene, this coefficient exhibits negligible changes once the pore size exceeds 10 nm.

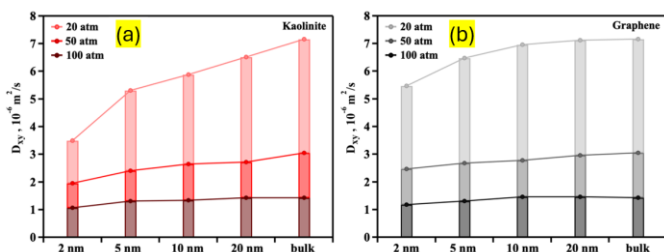


Figure 5. Lateral self-diffusion coefficients for H<sub>2</sub> in 2-20 nm (a) kaolinite (Al surface) and (b) graphene pores compared to those for bulk H<sub>2</sub> at pressures of 20, 50, and 100 atm.

- (2) Development of Non-reactive Vitrimer Model: As shown in Figure 6, the non-reactive vitrimer model does not express dynamic polymerization reactions between the two monomers, namely, bisphenol a diglycidyl ether (DGBEA) and 2-aminophenyl disulfide (AFD). The vitrimer model was generated by randomly mixing 296 DGEBA and 148 AFD monomers in a simulation box with an initial density of 0.3 g/cm<sup>3</sup>. Five MD simulations were performed with the NPT ensemble, where the temperature and pressure were maintained at 300 K and 1 atm, respectively. Each of those five simulations had a trajectory of 5 ns at the timestep of 1 fs. The inter- and intra-interactions were treated by the Polymer Consistent Force Field (PCFF), a Class II force field, using partial charges from the literature. The equilibrium vitrimer model has a density of 1.06 g/cm<sup>3</sup>, agreeing well with the 1.12 g/cm<sup>3</sup> literature report.

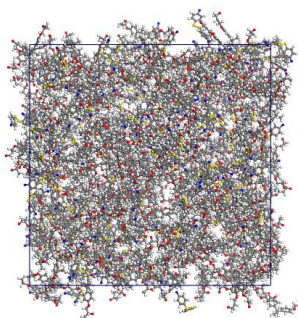
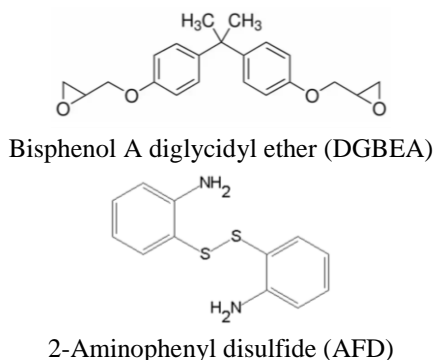


Figure 6. A non-reactive vitrimer model: **(Left)** Molecular structures of the two monomers, DGBEA and AFD; **(Right)** The final equilibrium structure of the vitrimer model, composed of 296 DGEBA and 148 AFD molecules, with a density of 1.06 g/cm<sup>3</sup> at 300 K and 1 atm.

**Task 3.4** Finite Element Numerical Analysis to Guide the Design of the Developed High-performance Healable CIPP Structural Liner (60%): During this reporting period, the research team (Dr. Chengcheng Tao, Junyi Duan, Ph.D. student from Purdue University) have conducted finite element analysis (FEA) for pipelines rehabilitated by CIPP liners as summarized below:

- (1) The Effect of Corrosion Hole Size on the Straight CIPP Liner System: Building on the previous report, Figure 7 shows the normalized stress of CIPP liner system with respect of corrosion hole size. The normalized stress is defined as the maximum stress normalized by the in-pipe pressure, and the hole size is dimensionless, obtained by dividing the hole radius ( $r$ ) by the pipe inner radius ( $R$ ) to unify the axes. The pipe normalized stress, with consideration of adhesive layer, decreases when the hole size ratio is small, and gets close to pipe without adhesive layer when the hole size ratio increases. Again, the normalized stress of liner decreases significantly with the presence of adhesive layer. Notably, the presence of a 1 mm adhesive layer significantly reduces liner stress, maintaining it within the ultimate strength range and stable across hole sizes.

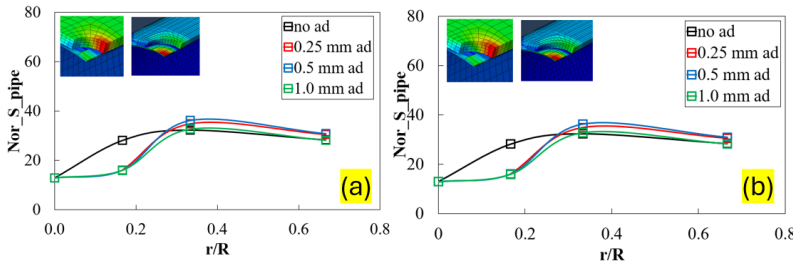


Figure 7. The normalized stress of CIPP liner system with respect of corrosion hole size. (ad = adhesive layer)

- (2) Elbow Pipes Protected by CIPP Liner Systems: Elbow pipes are typically categorized by the bend angle at which they redirect the flow of fluid. The most common angles for elbow pipe are 45 degrees and 90 degrees. Two degrees of elbows (45 and 90) and two radii of elbows (1D and 1.5D) are numerically investigated in this section. The dimensions and properties are detailed in Table 1. The results, as shown in Figure 8, indicate that the bending radius negatively affects the stress distribution on elbow pipe, whereas elbow angles have significantly less effect. The stress increments are 27.8% and 22.3% when decreasing the bending radius from 1.5D to 1D in 45-degree and 90-degree elbow pipes respectively. The stress is relatively stable when switch the elbow angles. The stress concentration zone is consistently found at the inner wall, with the difference being that the stress concentration zone grows with the increasing bending radius and elbow angles.

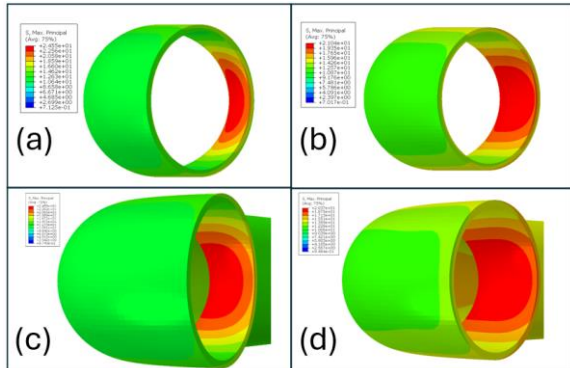


Figure 8. the distributions of maximum principal stresses on elbow pipes. (a) 45 degrees, 1D; (b) 45 degrees, 1.5D; (c) 90 degrees, 1D; (d) 90 degrees, 1.5D.

Table 1. The dimensions and properties of CIPP liner system.

Material	Parameter	Value
Cast-iron pipe	Length - $L_p$ (mm)	2400
	Thickness - $T_p$ (mm)	15
	Inner radius - $R_p$ (mm)	150
	Young's Modulus - $E_p$ (GPa)	100
	Poisson's ratio	0.3
Adhesive layer	Length - $L_A$ (mm)	Same as pipe
	Thickness - $T_A$ (mm)	0 ~ 1
	Inner radius - $R_A$ (mm)	150- $T_A$
	Young's Modulus - $E_A$ (GPa)	2
	Poisson's ratio	0.3
Starline® 2000 PSE-35 liner	Length - $L_L$ (mm)	Same as pipe
	Thickness - $T_L$ (mm)	3
	Inner radius - $R_L$ (mm)	150- $T_A$ - $T_L$
	Young's Modulus - $E_L$ (GPa)	0.4
	Poisson's ratio	0.4

**Task 4.1** Development of Embedded Distributed Fiber Optic Sensors for Self-sensing Structural Liner (60%), and **Task 4.2** Investigating the Load Transfer between Layers of the CIPP Liner and the Cast-iron Substrate (40%): During this reporting period, the research team (Dr. Ying Huang and Dr. Xingyu Wang) conducted an experimental study on corporation distributed fiber optic sensors to CIPP liner system and investigated the curing process and mechanism of adhesive layer; the sensor signals gathered from smart

liner system were utilized to create 2- and 3-D topographical views of the curing induced strain, the findings are presented below:

- (1) Investigation on Curing Process of Adhesive Layer by Using Smart Sensor-Liner System: The strain signals were collected over 5600 minutes, and the collected data includes every 0.65mm spot, the collected results was used to assist with understanding the curing kinetics of the adhesive layer. Additionally, both 2-D and 3-D plots visualizations were crafted for investigating the curing-induced strain effects on the liner system. Figures 9 (a) and (b) highlight the presence of non-uniform strain distribution across the liner, and the concentrated strain possibly attributed to the liner's geometry or the intrinsic material characteristics. A cross-sectional viewpoint along a single axis of the liner, at path 9, is depicted in Figure 9 (c), and Figures 9 (d) to (f) showcase the evolution of strain over the curing period at critical points identified in Figure 10 (c). Furthermore, Figure 9 (g) provides a visual depiction of the smart sensor-liner system, offering insights into the structure of the specimen under investigation.

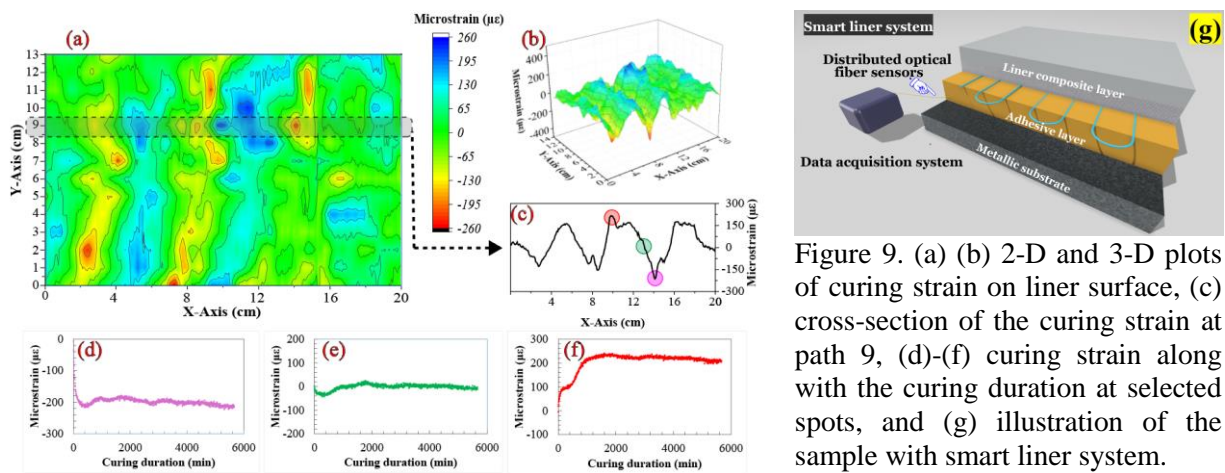


Figure 9. (a) (b) 2-D and 3-D plots of curing strain on liner surface, (c) cross-section of the curing strain at path 9, (d)-(f) curing strain along with the curing duration at selected spots, and (g) illustration of the sample with smart liner system.

- (2) Curing Kinetics Investigation for Adhesive Layer: The detection of non-uniform strain distribution across the liner suggests intricate patterns of strain evolution during the curing of the adhesive, potentially influenced by a variety of factors related to liner's geometric or material. In an effort to gain further insight into these curing strain dynamics, a sensor layer was positioned on the steel surface, as illustrated in Figure 10. A comparison of the strain data between the liner and steel reveals a pronounced difference in behavior, with the steel exhibiting a more consistent and less variable response to the curing process. This indicates that steel, unlike the liner material, does not undergo significant deformation transformation during curing.

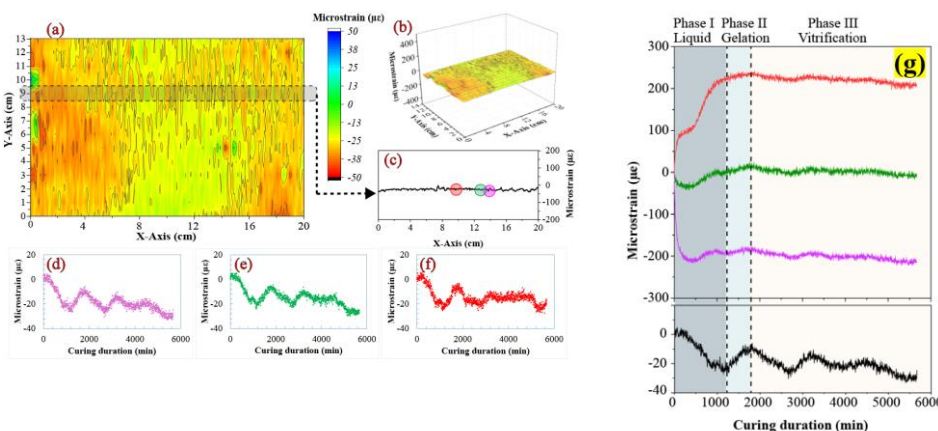


Figure 10. (a)-(f) curing strain on steel substrate, and (g) curing stage of the adhesive layer that identified by curing strain results, which obtained by smart liner system.

(3) Curing Stage Investigation for Adhesive Layer: Furthermore, the analysis of curing-induced strain signals within the smart liner system facilitates the monitoring of polymeric materials' curing stages. This is crucial for assessing the polymer's performance and determining when the liner is ready for service. Figure 10 (g) isolates three spots on the liner system that reflect varied final strain values after the curing process, characterized by positive (red line), negative (purple line), and near-zero (green line) strains. Additionally, a reference spot on the steel surface (black line) is selected. The curing process is segmented into three distinct phases: Phase I (liquid phase), Phase II (gelation phase), and Phase III (vitrification phase), and results showing that the smart liner system is capable of autonomously indicating when the adhesive reaches each of these curing stages.

**Task 5.1** Development of CIPP Liner Risk Index for the Pipeline Integrity Management Enhanced by AI Algorithms (40%): During this period, the research team (Dr. Chengcheng Tao, Yizhou Lin, Ph.D. student from Purdue University) have continued the multi-scale simulation for pipeline integrity management, with the results outlined below:

(1) Effect of Material Properties: In addition to the previous study, another single-parameter analysis evaluated the impact on isotropic fiber materials, focusing on epoxy's ultimate strain and Young's modulus. Findings presented in Figure 11 show that an increase in FM leads to heightened strength. Variations in the epoxy's EM and ES demonstrated a negligible effect on the composite's strength, whereas a higher FS marginally diminished the strength of the composite.

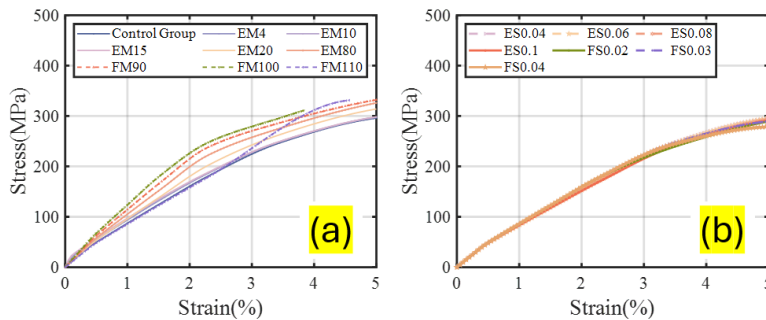


Figure 11. Stress-strain curve of fiber composite with material properties change (a) in Young's modulus; (b) in ultimate strain.

*Note: The baseline group: Epoxy with Young's Modulus (EM) of 3.35 GPa, Epoxy with ultimate strain (ES) at 0.02; Fiber Young's Modulus (FM) at 68.9 GPa, and Fiber ultimate strain (FS) at 0.016.*

(2) Dispersion Factor with Different fvfs & fiber Orientations: This analysis delved into the impact of fiber distribution within a composite on its properties, contrasting two distinct configurations: fibers aligned at a 0° orientation with a fiber volume fraction (fvf) of 1%, against a 45° orientation with a 2.5% fvf. Utilizing a Dispersion factor (d) to quantify dispersion effects, findings highlighted in Figure 12 (a) demonstrated that composites subjected to a higher concentration of fibers with less dispersion, as seen in the latter scenario, exhibited diminished strength, although the impact of dispersion on strength was comparatively marginal.

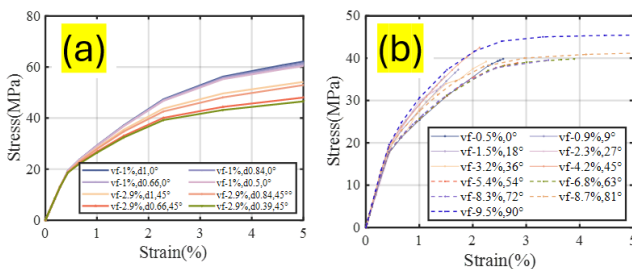


Figure 12. Stress-strain curve of fiber composite with (a) varied dispersion factors, and (b) varied fiber volume fraction and fiber orientation.

(3) Fiber Volume Fraction (fvf) with Fiber Orientation: The comprehensive bi-parametric examination of fiber volume fraction (fvf) and fiber orientation underscored that elevating both parameters simultaneously led to a consistent and stable enhancement in composite strength, as evidenced in Figure 12 (b). This indicated that fvf and the fiber orientation overall have an independent relationship.

### **Project Financial Activities Incurred during the Reporting Period:**

The cost breakdown during the reporting period in each category according to the budget proposal is shown in Table 2.

Table 2. Cost breakdown

Category	Amount spent during Q6
<b>Personnel</b>	
Faculty	\$0
Postdoc	\$7,649.99
Students (RA and UR)	\$12,128.08
Benefits	\$5,384.66
<b>Operating Expenses</b>	
Travel	\$1,280.28
Materials and Supplies	\$817.54
Recharge Center Fee	\$1,108
Consultant Fee	\$975
<b>Subcontracts</b>	\$5,709.37
<b>Indirect Costs</b>	\$13,204.66

### **Project Activities with Cost Share Partners:**

The Match fund from NDSU for this project is coming from the tuition of the associated graduate students during their work on this project. During the reporting period (Q6), Zahoor Hussain (100%), Muhammad Imran Khan (100%), Austin Knight (100%), and Tofatun Jannet (46.15%) were hired on the project. The tuition for the four students during Q6 was estimated to be \$12,520 at a rate of \$463.73 per credit.

### **Project Activities with External Partners:**

During this reporting period, George Ragula, our industry consultant, attended all the bi-weekly meetings with the research team.

### **Potential Project Risks:**

No potential risks were noticed during this reporting period.

### **Future Project Work:**

The research team will continue working on Tasks 2.1, 2.2, 3.1, 3.2, 3.3, 3.4, 4.1, 4.2 and 5.1.

### **Potential Impacts on Pipeline Safety:**

The newly developed self-healing epoxy demonstrates excellent compatibility with both liners and nanoparticles, yielding positive results in curing and self-healing processes. Further investigation into the properties of self-healing nanoparticle composites will be performed. Moreover, nanoparticles utilizing novel dispersion methods exhibit promise in enhancing polymeric composites with improved abrasion resistance and substrate adhesion/bonding. The integration of a smart sensor-liner system capable of monitoring strain history in the adhesive layer during curing, offering valuable insights for manufacturing specification development, quality control, and cure model validation. Ongoing analytical insights from studies on liner system modeling and fiber parameters provide essential guidance for future design and pipeline integrity management of liner systems. These findings not only benefit the project but also hold significance for the CIPP liner industry.